Structural and Vibrational Characterization of Tetracyanoethylene−Hexamethylbenzene as a Function of Pressure

Jennifer A. Ciezak*,†,‡ and Juscelino B. Leão†

NIST Center for Neutron Research, National Institute of Standards and Technology, Gaithersburg, Maryland 20899, and U.S. Army Research Laboratory, Weapons and Materials Research Directorate, Aberdeen Proving Ground, Maryland 21005

Received: November 3, 2005; In Final Form: January 17, 2006

The neutron powder diffraction and inelastic neutron scattering (INS) spectra of the electron donor−acceptor complex, tetracyanoethylene−hexamethylbenzene have been studied as a function of pressure to 0.414 GPa. Using the PW91 and PBE density functional theories, the unit cell vectors were calculated as a function of pressure and are compared to those experimentally obtained from the diffraction data. The calculated lattice vectors display large errors at low pressures but were found to be in close agreement with the experimental vectors at 0.414 GPa. Comparison of the experimental INS spectra of the TCNE−HMB enabled assignment of specific vibrational modes while providing a direct measurement of the effect of pressure on the complex. The PW91 vibrational frequency calculations reproduced both the vibrational intensities and frequencies with relative accuracy.

Introduction

The existence of several novel and unique physical properties of electron donor−acceptor complexes, such as magnetism,[1] conductivity, and superconductivity,[2] has generated considerable interest in recent years. It has been discovered that through control of external parameters such as temperature, pressure, and magnetic field strength, the magnitude of these properties can be tuned.[3] Although these materials are rapidly gaining extensive employment as integrated circuit components and sensors for mobile phones,[4] widespread potential exists for other applications. These complexes have been experimentally characterized for many years, yet much of the chemistry and physics of these materials that result in such unusual properties is just now being discovered. For new applications to emerge, it is necessary to first gain a deeper understanding of the fundamental characteristics of these materials, such as the relationship between intramolecular and intermolecular interactions, the internal conformation, relative orientation, and vibrational behavior.

Electron donor−acceptor (EDA) complexes are typically weakly interacting compounds that are formed when a donor molecule, *D*, donates an electron to an acceptor molecule, *A*.[3] The bonding arrangement in the solid-state is governed by electrostatic forces, and in most cases, the donor and acceptor molecules are arranged in stacks consisting of alternating donor and acceptor ions. The stacks are held together by weakly interacting van der Waals forces. The open-shell character of EDA complexes commonly results in electron−electron, electron−phonon, and spin coupling in the solid-state, as well as a variety of electronic instabilities, such as Mott, Peierls, and spin−Peierls transitions.[5] Although vast experimental knowledge about EDA complexes exists, theoretical descriptions remain rare and it is only in recent years several papers have appeared on the subject.[6−11]

Solid-state quantum chemical calculations are routinely used to examine the properties of solids, interfaces, and surfaces for a wide range of material classes and offer new hope in solving difficult quantum chemical problems that require more parameters than can be included in an isolated molecule simulation. By using a combined theoretical/experimental approach, the accuracy of these theoretical methods has greatly improved in recent years. Inelastic neutron scattering (INS) spectroscopy is a vibrational spectroscopic technique commonly employed as a fundamental test of theoretical methods. Inelastic neutron scattering spectra can be directly correlated to the normal mode eigenvectors, which are part of the standard output of an ab initio simulation. The large scattering cross-section of hydrogen can be exploited to obtain a vibrational spectrum that reveals primarily hydrogen motion. The intensity of all lattice and molecular vibrations observed in the spectrum is directly proportional to the sum of the squares of the hydrogen displacement vectors for a particular normal mode of vibration. Numerous recent investigations comparing INS vibrational and theoretical spectra exist, including a recent report on an EDA complex formed between tetracyanoquinodimethane (TCNQ) and hexamethylbenzene.[11−19]

The focus of this work concerns the electron donor−acceptor complex formed between tetracyanoethylene and hexamethylbenzene (TCNE−HMB), shown in Figure 1. At room temperature, X-ray diffraction shows equally spaced TCNE and HMB molecules arranged in a DADADA arrangement with an intermolecular spacing of 3.35 Å.[20] This spacing decreases to 3.28 Å at 113 K.[21] The TCNE−HMB complex has been subject to extensive experimental characterization using X-ray diffraction,[20,21] optical absorption spectroscopy,[22−24] infrared spectroscopy,[25−30] Raman scattering[31−37] and most recently, inelastic neutron scattering.[10] Several attempts have been made to obtain an accurate theoretical representation of the complex, but many

* Corresponding author. Address: 100 Bureau Dr., MS 8562, Gaithersburg, MD 20899. Tel: (301) 975-6082. Fax: (301) 921-9847. E-mail: jciezak@arl.army.mil.

† National Institute of Standards and Technology.

‡ U.S. Army Research Laboratory, Weapons and Materials Research Directorate.

10.1021/jp056351n
Published on Web 02/15/2006

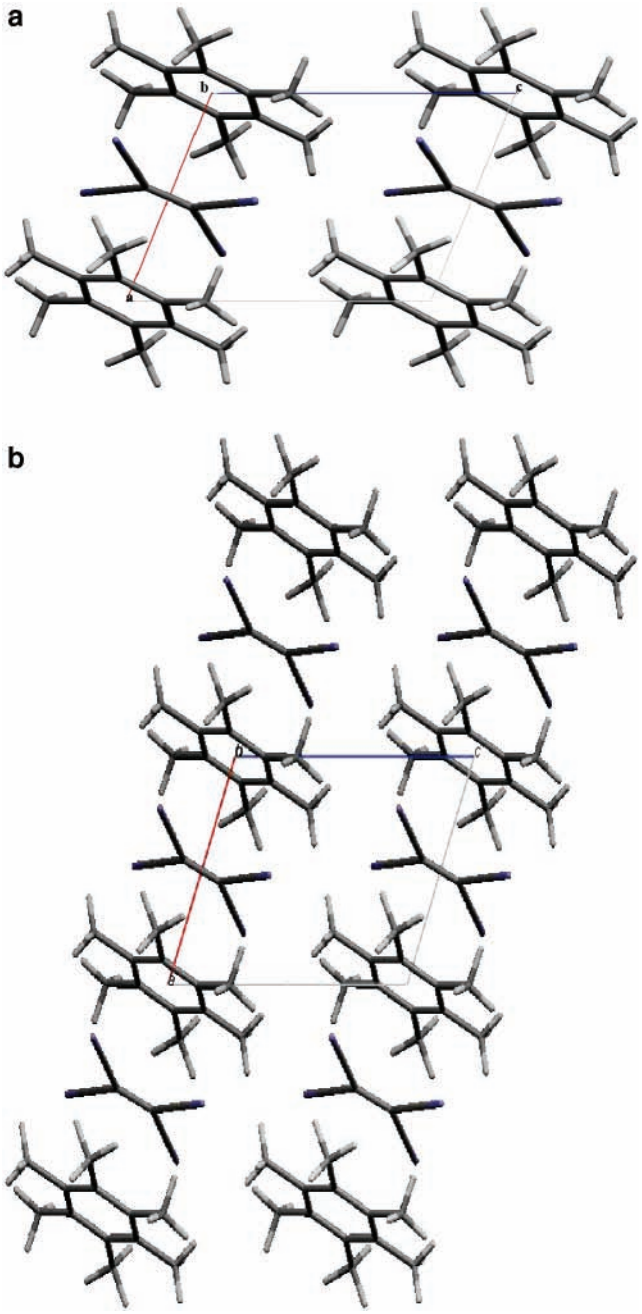

Figure 1. Molecular geometry of the TCNE−HMB complex shown (a) in the unit cell and (b) as an expanded view showing the stacking arrangement.

of these studies have been limited due to use of an isolated complex as the model for the simulations.[9,28,38] Recent solid-state calculations have demonstrated the importance of including the intermolecular interactions to obtain an adequate description of the TCNE−HMB complex.[10]

Optical absorption[39−44] and infrared spectroscopy[44,45] have been used to characterize pressure-induced changes of the TCNE−HMB complex in solution and the solid-state, respectively. Optical spectra obtained as a function of pressure indicated an increase in the ionic character of TCNE−HMB.[39−44] This is corroborated with the IR data that showed all vibrational frequencies linearly increase as a function of pressure.[44,45] Interestingly, the intensity of the C═C (A_g) band of TCNE increased almost 5 times between 0 and 10 GPa. The increase in intensity as a function of pressure for this particular vibration was proposed to be due to a subtle shift of the TCNE molecule from the site symmetry occupied in the atmospheric pressure crystal structure.[45] This shift was expected to be at, or near, the resolution limit of the X-ray diffraction structure; thus no crystallographic analysis was undertaken at that time. As such, it seems justified to seek an understanding of the pressure dependent physical properties of the TCNE−HMB complex.

We report here the results of neutron diffraction, inelastic neutron scattering, and theoretical studies of TCNE−HMB compressed to 0.414 GPa at 50 K. Our neutron diffraction studies to 0.414 GPa show a much higher compression of the *b* axis, relative to the *a* and *c* axes. Large errors are observed in the calculated unit cell vectors, which systematically decrease as the pressure increases. Presumably, these errors in the unit cell vectors reflect the lack of van der Waals' forces implemented in current density functional theory (DFT) functionals. This phenomenon has also been reported during crystal structure predictions of energetic materials.[46] Vibrational modes for the solid-state TCNE−HMB complex under pressure were generated using density functional theory ab initio quantum mechanical calculations. Good correspondence between the calculated modes and experimentally obtained spectra allowed the assignment of vibrational modes to the experimentally observed INS peaks.

Materials and Methods

Experimental Details. Tetracyanoethylene and hexamethylbenzene were obtained from Sigma Aldrich and used without further purification. The EDA complex, TCNE−HMB, was synthesized according to previously published methods.[21] Approximately 1.5 g of the TCNE−HMB complex was ground into a fine powder and loaded into a cylindrical aluminum pressure cell and placed into a top-loading cryostat. The polycrystalline powder was held at 50 K for the duration of the experiments. The pressure cell used for these experiments is constructed from a 40 mm diameter cylindrical piece of aluminum and is able to reach a maximum pressure of 0.414 GPa. The sample compartment is a cylindrical opening 5 mm in diameter and 45 mm long. One end of the cell is sealed using a steel ball and screw mechanism and the other end is connected to the pressure intensifier by a stainless steel capillary. Specific details concerning the method for pressurizing the cell can be found at the NIST Center for Neutron Research website.[47]

Neutron Powder Diffraction. Angle-dispersive neutron powder diffraction experiments, using a neutron wavelength of 1.5402 Å, were carried out at the BT-1 thirty-two-detector neutron powder diffractometer at the National Institute of Standards and Technology Center for Neutron Research (NCNR) in Gaithersburg, MD. The Cu (311) monochromator was employed for all of the experiments described herein and data were collected over the range 3−168° 2θ for approximately 24 h at each pressure.[48] The General Structure Analysis program[49] graphical user interface EXPGUI[50] employing Rietveld refinement was used to obtain the unit cell parameters in the 5−36° 2θ and 46−165° 2θ ranges. Diffraction between 36° and 46° 2θ is dominated by two intense aluminum diffraction peaks, which represent the (001) and (111) crystal planes of the pressure cell. The parameters used for the initial refinement of the TCNE−HMB complex at atmospheric pressure and 50 K were obtained from the Cambridge Structural Database and are as follows: space group = $P\bar{1}$, $a = 6.563$ Å, $b = 8.614$ Å, $c = 8.656$ Å, $\alpha = 108.22°$, $\beta = 102.61°$, $\gamma = 111.74°$, $Z = 1$. At all other pressures, the initial refinement parameters were the final results obtained in refining the diffraction pattern of the next lower pressure.

Inelastic Neutron Scattering. Inelastic neutron scattering spectra were collected between 40 and 1200 cm^{-1}, on the Filter Analyzer Neutron Spectrometer (FANS) located at BT-4 at the NIST Center for Neutron Research, through the use of both the copper (Cu (220)) and pyrolytic graphite (PG (002)) monochromators. The scattered neutrons were collimated with 20/20 min of arc divergence prior to inelastic scattering by the sample. The scattered neutrons first passed through a bismuth filter that removes any spurious Be-phonon excitations and then Bragg cutoff filters of polycrystalline beryllium and graphite that remove all neutrons with energy greater than 1.8 meV. Though the FANS instrument is capable of scanning from ~32 to 1700 cm^{-1}, this experiment focuses only on the 40−1200 cm^{-1} range. More specific details are available regarding the FANS instrument.[51] All experimental INS spectra presented in this paper were normalized for background scattering using the Data Analysis and Visualization Environment (DAVE) program.[52]

Computational Details. The calculated crystal parameters and normal modes of vibrations were obtained as a function of pressure using the Vienna Ab Initio Simulation Package (VASP).[53] The lattice parameters were obtained as a function of pressure using both the Perdew−Burke−Ernzerhof (PBE)[54] and Perdew−Wang 91 (PW91)[55] functionals. Only the vibrational results using the PW91 functional are presented here, as we were unable to obtain reliable vibrational frequencies using the PBE functional. Vanderbilt ultrasoft pseudopotentials (USP)[56] and Monkhorst−Pack *k*-point generation methods were used for all calculations. Calculations were run at 280, 330, 430, 495, 545, and 645 eV to test for convergence, which was noted at 545 eV.

In all calculations, no symmetry restrictions were imposed. At atmospheric pressure, the calculations were started from the unit cell and structural parameters listed in the Cambridge Structural Database.[21] The electronic energies were allowed to converge to 2.0×10^{-6} eV and the structure was considered converged once the difference in free energy between gradient steps was less than 2.0×10^{-5} eV. Calculations were done at 0.138, 0.276, and 0.414 GPa to coincide with our experimental measurements. These calculations were started from the optimized structures obtained from optimizing the structure of the next lowest pressure. The optimized molecular geometries were then used to determine the Hessian matrix and the vibrational frequencies of the TCNE−HMB complex via the finite difference method. The theoretical inelastic neutron scattering spectra were constructed from the normal mode eigenvectors using the A-Climax program v.5.1.3.[57,58]

Results and Discussion

Unit Cell. Neutron diffraction patterns were obtained for the TCNE−HMB complex as a function of hydrostatic pressure to 0.414 GPa. Because only the first twenty peaks of the experimental data were available for refinement, it was not possible to assign the atomic coordinates to each molecule in the asymmetric unit cell using Rietveld analysis. Therefore, we will not discuss the accuracies of the calculated molecular geometries. Instead, this section will focus on the accuracy of the calculated unit cell parameters as a function of pressure.

The experimental unit cell parameters are reported in Table 1 as a function of pressure. The unit cell parameters and volume obtained at 50 K (0 GPa) are similar to the parameters and volume reported at 113 K.[21] The volume decreases by 0.24% upon cooling from 113 to 50 K. As expected, the overall experimental volume of the unit cell decreased with increasing pressure from 398.626 $Å^3$ at 50 K (0 GPa) to 377.221 $Å^3$ at

TABLE 1: Unit Cell Parameters of TCNE−HMB at 113 K[20] and as a Function of Pressure at 50 K As Determined in This Study

	113 K[21]	0 GPa (50 K)			0.138 GPa (50 K)			0.276 GPa (50 K)			0.414 GPa (50 K)		
param	exp	exp	PBE	PW91	exp	PBE	PW91	exp	PBE	PW91	exp	PBE	PW91
a (Å)	6.563(2)	6.563(1)	7.214(5)	6.987(0)	6.560(3)	7.044(1)	6.908(0)	6.487(4)	6.617(2)	6.542(8)	6.465(1)	6.433(1)	6.460(4)
b (Å)	8.614(2)	8.634(0)	8.896(3)	8.716(3)	8.632(5)	8.941(6)	8.833(3)	8.492(9)	8.861(6)	8.772(1)	8.365(6)	8.325(2)	8.350(9)
c (Å)	8.656(1)	8.638(3)	8.938(2)	8.891(7)	8.634(2)	8.821(0)	8.714(5)	8.516(6)	8.690(1)	8.616(3)	8.509(2)	8.472(9)	8.497(9)
α (deg)	108.22(2)	108.294(5)	108.015(1)	108.327(1)	108.292(0)	108.306(7)	108.296(1)	107.530(1)	107.535(2)	107.527(1)	106.993(2)	106.989(8)	106.999(1)
β (deg)	102.61(2)	102.682(6)	102.737(8)	102.694(3)	102.672(6)	102.679(4)	102.665(3)	103.128(1)	103.126(7)	103.124(4)	103.506(3)	103.501(3)	103.503(3)
γ (deg)	111.74(2)	111.804(3)	111.820(5)	111.806(6)	111.806(2)	111.814(3)	111.813(6)	111.381(6)	111.375(4)	111.379(2)	111.766(5)	111.771(6)	111.757(2)
vol ($Å^3$)	399.597	396.882	468.427	441.058	397.723	452.639	433.332	385.330	418.609	380.416	377.002	371.943	375.725

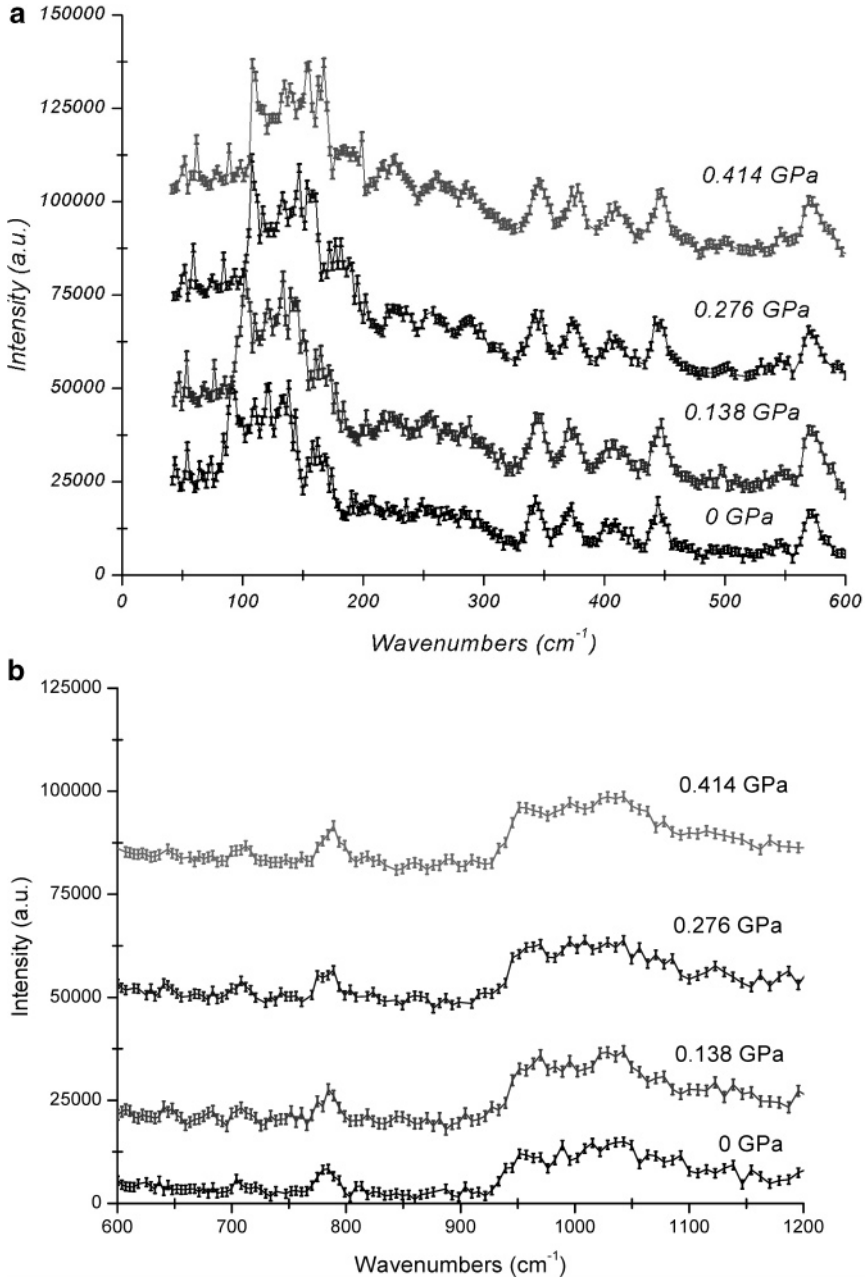

Figure 2. Experimental INS spectra of the TCNE−HMB complex collected on the FANS instrument at 50 K in the spectral ranges (a) 0−600 cm^{-1} and (b) 600−1200 cm^{-1}. Spectra are shown as a function of pressure and are offset for ease of comparison.

0.41 GPa. This corresponds to a 5.37% decrease in the volume of the unit cell. As is shown in Table 1, the compression of the *b* axis increased sharply between 0.138 and 0.276 GPa in comparison to the *a* and *c* axis. The higher compression exhibited by the *b* axis implies that the entire unit cell compresses anisotropically. This effect is not uncommon in layered materials, and in the TCNE−HMB complex the *b* axis lies in the direction perpendicular to the stacked layers. These layers are held together only by weak van der Waals' interactions. Therefore, one would expect the *b* direction of the unit cell to be much more compressible than either the *a* or *c* direction of the unit cell.

The calculated unit cell parameters as a function of pressure using the PBE and PW91 methods are summarized in Table 1. The observed errors for the experimental lattice parameters derived as a function of pressure are provided in the Supporting Information, Table S1. Comparison of the calculated unit cell parameters and the experimental parameters reveals large errors using both functionals. The RMS values at 0 GPa (50 K) are 0.333 (PBE) and 0.205 (PW91). The RMS values decreased slightly to 0.246 (PBE) and 0.167 (PW91) at 0.138 GPa. The RMS values systematically declined as the pressures increased, with values of 0.175 (PBE) and 0.124 (PW91), at 0.276 GPa. At 0.414 GPa, the calculated parameters were in close agreement with the experimental parameters and the RMS deviations are 0.026 (PBE) and 0.009 (PW91). The magnitude of the errors in the calculated cell vectors is clearly reflected in the RMS deviations between the experimental and calculated volumes. The PBE method yielded volume measurements with percent errors of 18.2% (0 GPa), 12.9% (0.138 GPa), 8.6% (0.276 GPa) and 1.3% (0.414 GPa). Slightly smaller RMS deviations in the cell volume were obtained with the PW91 method. The RMS deviations were 11.3% (0 GPa), 8.9% (0.138 GPa), 1.3% (0.276 GPa) and 0.3% (0.414 GPa) with the PW91 method.

It has been proposed that overestimation of lattice vectors arises from lack of proper van der Waals forces in current DFT

TABLE 2: Experimental Peak and Theoretically Determined Vibrational Mode Energies of the TCNE−HMB Complex, Corresponding to Peaks Observed in the INS Spectra between 40 and 1200 cm^{-1} Collected under Both Ambient and Pressurized Conditions at 50 K Using the FANS Instrument[a]

0 GPa		0.138 GPa		0.276 GPa		0.414 GPa			
INS	PW 91	INS	PW 91	INS	PW 91	INS	PW 91	mode no.[b]	molecular motion
	5		7		8		12	1	HMB−TCNE twisting
	30		35		40	51	52	2	HMB−TCNE sliding
44	40	54	56	52	58	58	58	3	HMB−TCNE stretching
54	60	NR	57	59	60	62	62	4	HMB−TCNE tilting
64	64	67	67	75	73	78	75	5	HMB−TCNE tilting
73	79	77	76	84	81	89	86	6	HMB−TCNE tilting
85	82	96	96	94	99	97	99	7	HMB CH_3 twist and TCNE C−C≡N out-of-plane torsion
91	93	102	104	107	108	108	112	8	HMB CH_3 twist and TCNE C−C≡N out-of-plane torsion
99	101	110	109	116	117	116	125	9	HMB CH_3 twist and ring deformation
108	110	127	126	133	135	135	131	10	C−C≡N bend
121	120	134	133	142	145	141	146	11	Methyl torsion
133	137	140	145	147	149	154	156	13	C−C≡N bend
138	143	145	146	153	153	NR	157	14	methyl torsion and C−C≡N in-plane torsion
145	150	151	147	158	163	161	161	15	methyl torsion
155	154	156	157	167	168	167	168	16	TCNE scissor mode
158	157	161	160	172	182	177	176	17	methyl torsion
163	159	165	162	177	184	181	183	18	C≡N bend and $2\nu_8$
169	168	172	173	181	185	190	192	19	methyl torsion
174	170	177	178	188	186	NR	193	20	methyl torsion
190	182	200	197	195	196	199	198	22	ring deformation
193	193	203	200	202	204	205	205	23	ring deformation
208	208	206	210	212	215	217	217	24	CH_3 torsion
220	218	221	222	224	227	226	226	25	ring deformation and CH_3 torsion
226	227	NR	228	228	230	230	231	26	ring $-CH_3$ bending out-of-plane
236	235	236	235	236	239	238 (sh)	237	27	ring $-CH_3$ bending out-of-plane
249	249	245	250	251 (sh)	253	251 (sh)	250	28	C−C≡N bend
256	255	266	256	258	261	260	260	29	ring $-CH_3$ bending in-plane
269	267	271	263	NR	267	271	272	30	ring $-CH_3$ bending out-of-plane
284	282	281	279	284	282	286	284	31	ring $-CH_3$ bending in-plane
288	288	288	286	288	289	291	290	32	ring $-CH_3$ bending in-plane
302 (sh)	301	299	303	NR	295	306	304	33	C−C≡N bend
314	313	314	317	314 (sh)	311	316	318	34	C−C≡N bend
321	321	326	327	331	327	341 (sh)	340	36	C−C−C rocking (TCNE)
340 (sh)	339	344 (sh)	341	343	340	347	347	35	methyl torsion
343	344	347	347	352	350	352 (sh)	352	37	methyl torsion
360	357	362 (sh)	359	363	364	365 (sh)	368	38	ν_{18} benzene-like mode Wilson scheme
367 (sh)	366	368	363	NR	371	373	372	39	C−C≡N bend
373	375	375	382	378	382	378	381	40	C−C≡N bend
380 (sh)	378	396 (sh)	394	396	393	396 (sh)	395	41	Methyl torsion
401	399	401	400	404	401	404	403	42	methyl torsion
409	408	409	414	409	409	409	411	43	out-of plane ring deformation
417	416	425 (sh)	424	425	425	428	428	44	in-plane ring deformation
423	425	430	433	441	437	NR	441	45	C−C−C rocking (TCNE)
444	446	447	448	447	446	447	449	46	C−CH_3 deformation
467	466	469	467	473 (sh)	471	476	475	47	out-of plane ring deformation
479	480	481	483	484	488	487	484	48	in-plane ring deformation
487	486	487	489	490 (sh)	496	499 (sh)	497	49	C−C−C rocking (TCNE)
494	492	496	500	502	500	NR	510	50	C−C−C wagging (TCNE)
520	518	517	519	NR	521	517	518	51	C−C−C bend
533	534	533	534	530	533	527	532	52	C−C≡N bend
546	545	546	543	546	549	546	547	53	C−C−C bending (TCNE)
572	574	572	570	569	573	578	575	54	C−C−C wagging (TCNE)
586 (sh)	588	589	593	593	596	589 (sh)	583	55	C−C stretch (TCNE)
600	602	610	607	614	612	615	617	56	CH_3 out-of-plane deformation
637	639	640	646	640	646	644	649	57	ν_{12} wilson benzene
667	665	667 (sh)	663	671	668	671	675	58	C≡N stretch
683	685	683	677	683	682	683	689	59	C≡N stretch
704	703	708	699	708	703	712	719	60	C≡N stretch
720	720	733	726	734	739	738	740	61	ring breathing
738	736	742	741	742	750	747	755	62	C−C−C wagging (TCNE)
756	755	760	761	756	762	760	767	63	C−C stretch (TCNE)
774 (sh)	771	774	769	775	778	779 (sh)	782	64	ring breathing
784	787	784	783	788	789	789	791	65	CH_3 out-of-plane deformation
810	812	818	814	823	829	829	827	66	rocking CH_3 in-plane
844	842	844	845	859	851	860	858	67	rocking CH_3 out-of-plane
856	855	870	865	871	872	876	878	68	bending CH_3 out-of-plane
876 (sh)	878	882	884	887	891	893	895	69	bending CH_3 in-plane

TABLE 2 (Continued)

0 GPa		0.138 GPa		0.276 GPa		0.414 GPa			
INS	PW 91	INS	PW 91	INS	PW 91	INS	PW 91	mode no.[b]	molecular motion
887	885	904	900	898	906	909	911	70	CH_3 out-of-plane deformation
916	915	927	927	930 (sh)	922	933 (sh)	927	71	bending CH_3 in-plane
939	940	951	942	951 (sh)	944	NR	957	72	C≡N stretching (TCNE)
970	971	970	966	970	974	NR	984	73	C−CH_3 stretch and CH_3 deformation
989	984	995	992	996	996	996	998	74	ν_{14} benzene-like mode Wilson scheme
1015	1015	1022	1025	1029	1030	1029	1031	75	rocking CH_3 out-of-plane
1042	1043	1043	1039	1043	1040	1043	1043	76	rocking CH_3 in-plane
1050 (sh)	1050	1056 (sh)	1051	1070	1067	1078	1079	77	rocking CH_3 in-plane
1065	1065	1078	1075	1085	1085	1100	1106	78	ν_{20} benzene-like mode Wilson scheme
1072 (sh)	1073	1085	1089	1107 (sh)	1100	1110	1118	79	bending CH_3 out-of-plane
1155	1157	1178	1180	1187	1188	NR	1188	80	C≡N stretching

[a] The assignments of the molecular motions are similar to that previously reported.[10] [b] Molecular modes are numbered according to ref 10.

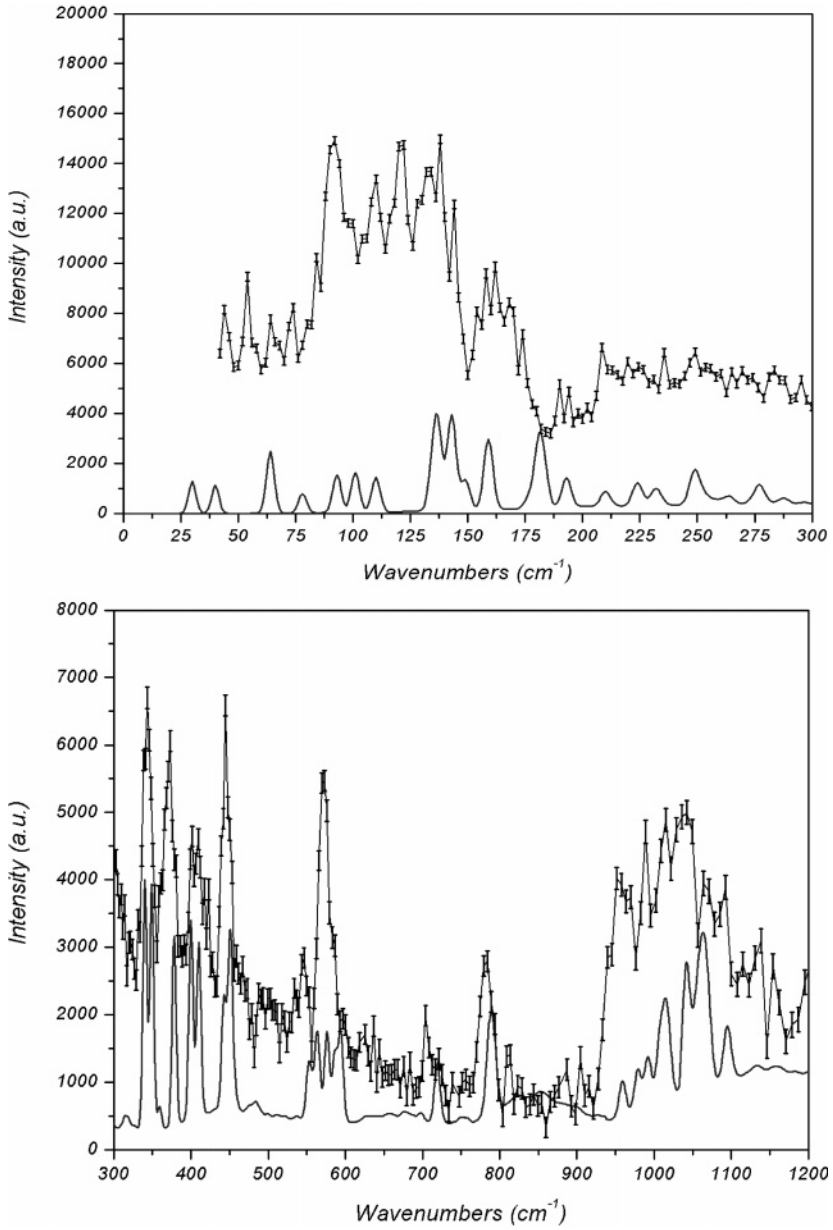

Figure 3. Comparison of the experimental INS spectrum at 50 K (0 GPa), shown with experimental error bars, and the calculated INS spectrum (solid line) shown in the (a) the 0−300 cm^{-1} and (b) 300−1200 cm^{-1} spectral ranges. Spectra are offset for ease of comparison.

functionals.[46] In the case of the TCNE−HMB complex, the largest error in the individual lattice vectors is observed for the *b* lattice parameter. Along the *b* axis, as previously discussed, van der Waals forces are largely responsible for holding the crystal together. As pressure increases, the error decreases because the stacks are forced into a closer packed arrangement and the electron densities begin to overlap. Both the *a* and *c* lattice vectors systematically decrease as pressure increases.

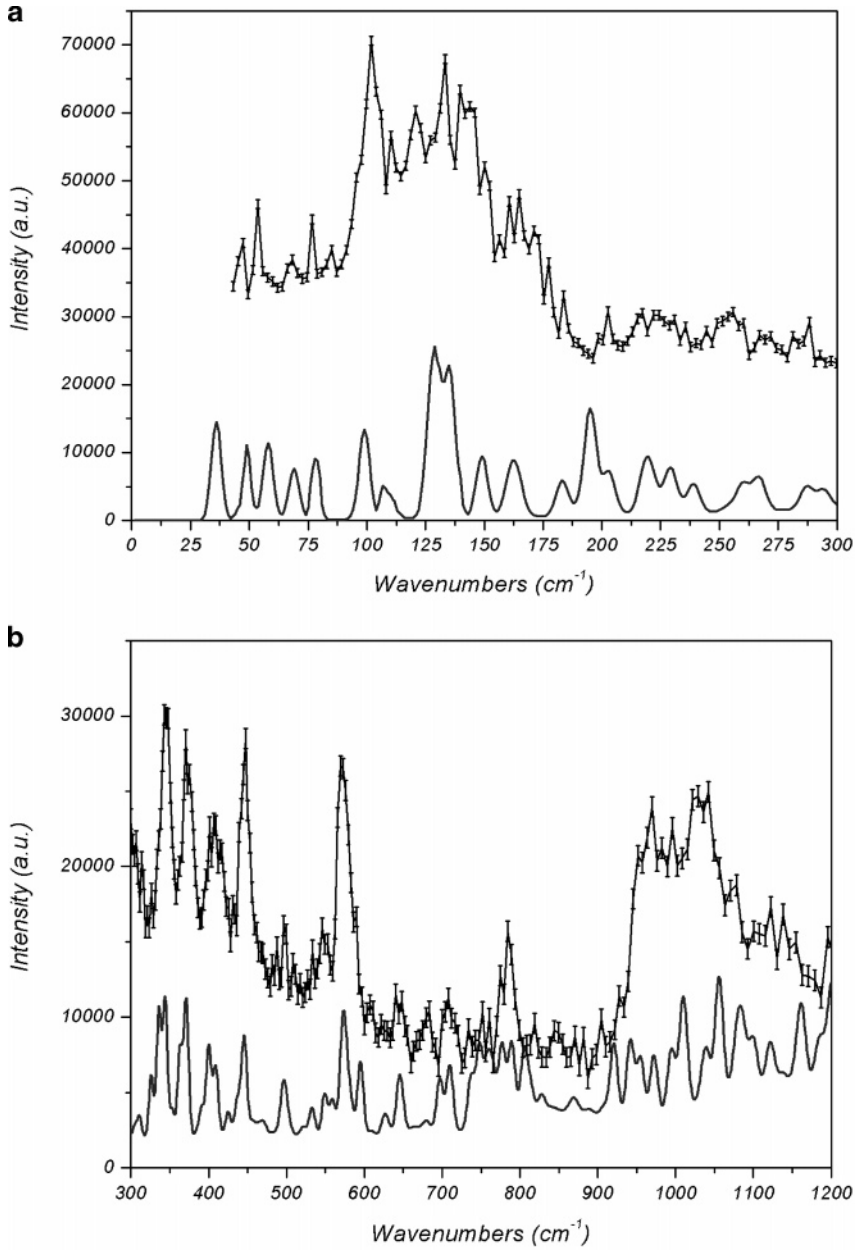

Figure 4. Comparison of the experimental INS spectrum at 0.138 GPa, shown with experimental error bars, and 50 K and the calculated INS spectrum (solid line) shown in the (a) 0−300 cm^{-1} and (b) 300−1200 cm^{-1} spectral regions using the PW91 functional. Spectra are offset for ease of comparison.

Although the calculated *b* lattice vector slightly increases in length between 0 and 0.138 GPa, this correctly models the experimental behavior. Above 0.138 GPa, the length of the *b* vector decreases. At 0.414 GPa, the values of all lattice parameters agree relatively well with experiment.

Molecular Vibrations. The inelastic neutron scattering spectra of the TCNE−HMB complex obtained at 50 K are shown in Figure 2 as a function of pressure. The spectra are offset for ease of comparison. At low frequency, in the spectral range of 40−300 cm^{-1}, the INS spectra are characterized by several strong vibrational modes atop a broad envelope of intensity, which tails off to higher frequency. As is shown in the literature, this vibrational pattern is characteristic of hexamethylbenzene, which has several intense methyl torsions and phonon modes in this vibrational region.[58]

The center of the broad band at 0.414 GPa is not noticeably shifted relative to that at 0 GPa, but it can be shown through close examination of Table 2, which details the vibrational assignments of the TCNE−HMB complex as a function of pressure, that several vibrational modes, in particular methyl torsions, have large vibrational shifts of 15 cm^{-1} or more. The two intense bands at 121 and 169 cm^{-1} in the 0 GPa spectrum correspond to those at 141 and 190 cm^{-1} in the 0.414 GPa spectrum, with vibrational shifts of 20 and 21 cm^{-1}, respectively. Large red shifts have been suggested to result from of an increase in the ionic character of the EDA complex and the existence of a phase transition, termed the neutral-to-ionic transition, has been reported at higher pressures for several EDA complexes.[59] In contrast to the large vibrational shifts at 120 and 169 cm^{-1}, the two methyl torsion modes ca. 220 cm^{-1} (0 GPa) and 401 cm^{-1} (0 GPa), are only slightly affected by pressure application and vibrational shifts of only 3−6 cm^{-1} are observed. These relatively small shifts can likely be attributed to the intrinsic width of these vibrational bands in the INS spectra, as a result of overlapping of the fundamental

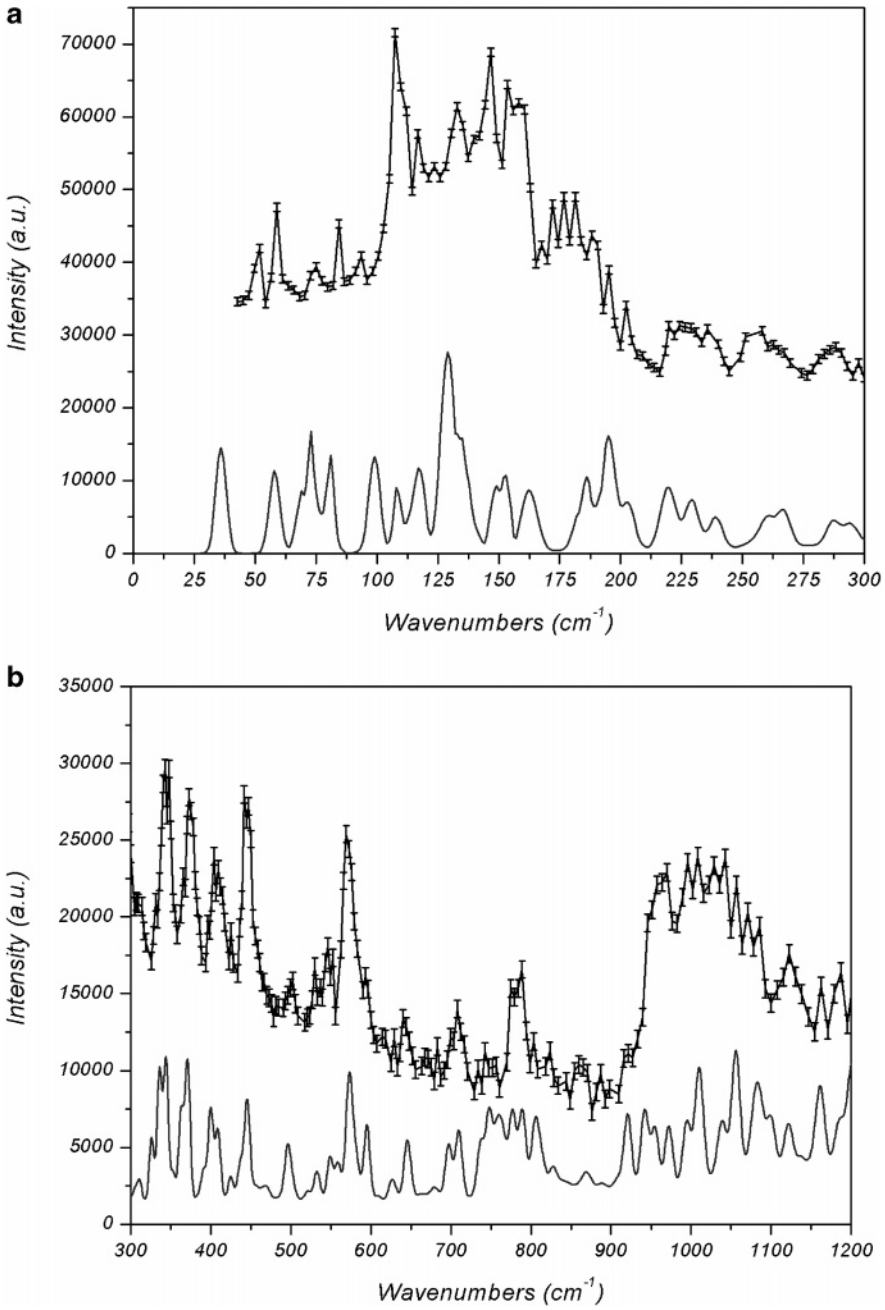

Figure 5. Comparison of the experimental INS spectrum at 0.276 GPa, shown with experimental error bars, and 50 K and the calculated INS spectrum (solid line) using the PW91 functional shown within the (a) 0−300 cm^{-1} and (b) 300−1200 cm^{-1} spectral ranges. Spectra are offset for ease of comparison.

vibrations with combination and overtone bands, leading to a smaller peak shift than is actually present.

Slight differences in the vibrational patterns as a function of pressure are also observed in the regions near 350, 375, and 440 cm^{-1}. The relatively intense broad peak attributed to two methyl torsions ca. 340 and 343 cm^{-1} at 0 GPa split into two distinct bands at a pressure of 0.276 GPa. The two methyl torsions at 373 cm^{-1} (0 GPa) and 380 cm^{-1} (0 GPa), which appear as a single strong band near 375 cm^{-1}, also show splitting at 0.138 and 0.414 GPa. The evolution of the vibrational modes between 340−350 and 370−380 cm^{-1} as a function of pressure is a direct result of the changing geometry of the methyl groups. As pressure increases, the staggered arrangement of the methyl groups, which is found at ambient conditions, becomes more pseudoplanar in nature. This, in turn, results in differing degrees of vibrational shifts. The vibration near 440 cm^{-1} can be attributed to a methyl deformation, which shows slight evidence of vibrational splitting at 0.276 GPa. Because no other vibrational modes are found in close proximity, factor group splitting could cause the splitting of this vibrational band, as symmetry related methyl groups are forced to reside in different environments as pressure increases.

DFT Calculations. The INS experimental frequencies and calculated vibrational frequencies were used to investigate the symmetries associated with the pressure-induced changes observed in the TCNE−HMB complex. Table 2 presents a comparison of the observed and calculated frequencies of the TCNE−HMB complex as a function of pressure. Descriptions of the molecular motion for the normal modes in the region studied are also presented in Table 2. These assignments of molecular motion are in close agreement with previously published data[10] and the INS vibrational frequencies calculated

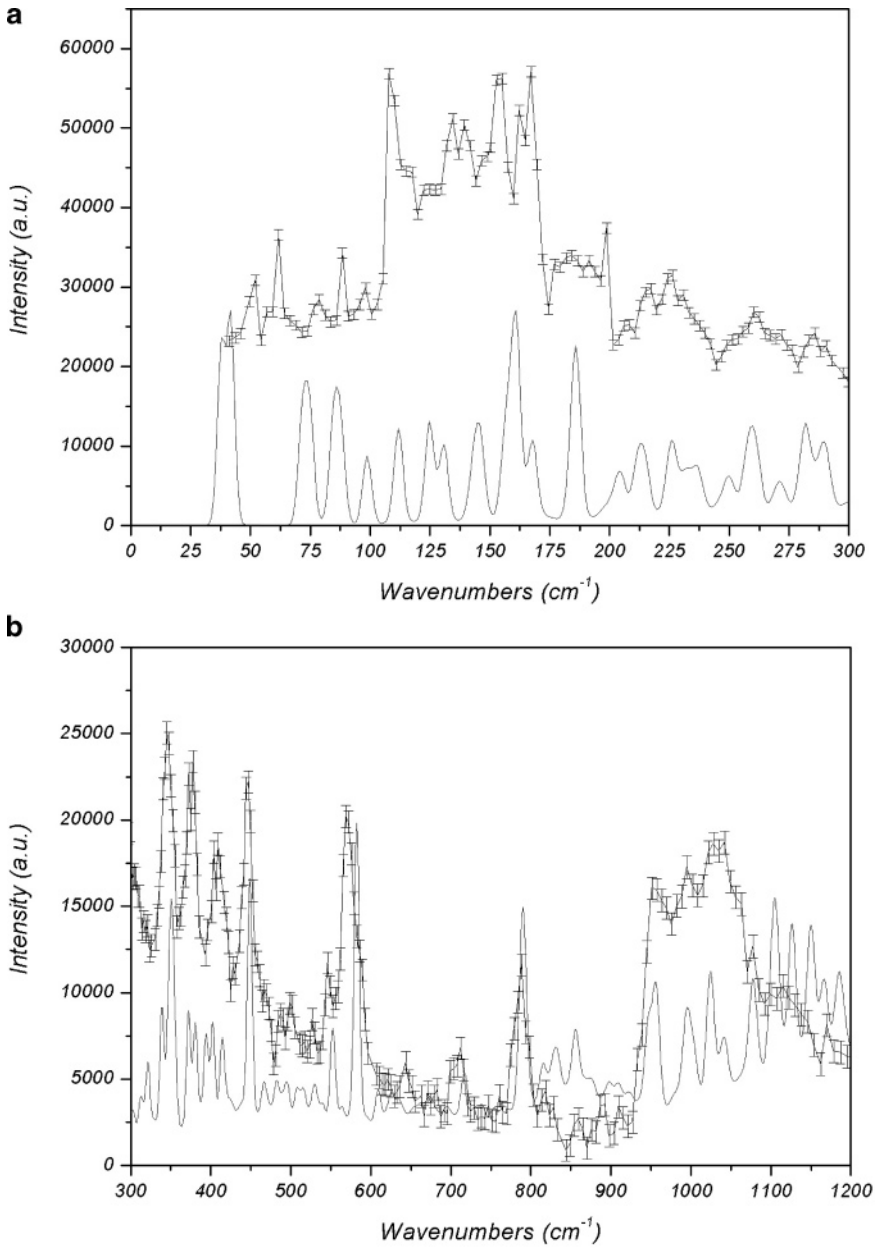

Figure 6. Comparison of the experimental INS spectrum, shown with experimental error bars, at 0.414 GPa and 50 K and the calculated INS spectrum (solid line) in the (a) 0−300 cm^{-1} and (b) 300−1200 cm^{-1} spectral regions. Spectra are offset for ease of comparison.

with the PW91 functional closely model the experimental INS data for all pressures studied. At 0 GPa, the rms value is 2.41 cm^{-1}. The corresponding rms value at 0.138 GPa is 3.68 cm^{-1}. The rms value increased slightly to 4.03 and 3.31 cm^{-1} at 0.276 and 0.414 GPa, respectively.

Individual comparisons of the experimental and calculated INS spectra are shown in Figures 3−6 as a function of pressure. A comparison of Figures 3 and 6 shows the intensities of the calculated INS spectra change significantly upon pressure increase, while the intensities of the experimental spectra remain virtually the same. This is particularly apparent in the spectral region between 800 and 900 cm^{-1}, a region that is characterized by several out-of-plane motions of the methyl groups. Because the intensity of an INS transition is dependent upon hydrogen displacement, an increase in calculated intensity indicates the calculated molecular geometry is slightly different from the true crystal structure. However, this can only be confirmed through a high-resolution crystallographic analysis, which is beyond the scope of this paper.

A comparison of the calculated and experimental frequencies summarized in Table 2 and Figures 3−6 reveals, in general, good frequency and intensity agreement between calculation and experiment. The calculations presented in this paper are somewhat limited in the sense that they do not include vibrational intensity from the external lattice modes of the complex, which is reflected by the absence of strong phonon bands below 200 cm^{-1}. To further improve upon the agreement of calculation and experiment, it will be necessary to perform a full crystal calculation on a "supercell".

Six intermolecular vibrational modes were predicted for each pressure. The HMB−TCNE stretching vibration was predicted at 40 cm^{-1} at 0 GPa and was experimentally observed at 44 cm^{-1}. Under pressure, the vibration experimentally red-shifted to 58 cm^{-1}, with a calculated value of 58 cm^{-1}. Three HMB−TCNE tilting modes were experimentally observed at 54, 64, and 73 cm^{-1} at 0 GPa, with calculated counterparts of 60, 64, and 79 cm^{-1}, respectively. These vibrations, at 0.414 GPa, shifted to 62, 78, and 89 cm^{-1} with calculated values of 62, 75,

and 86 cm^{-1}, respectively. The intermolecular modes of EDA complexes are highly coupled to the degree of electron transfer and such large red shifts indicate an increase in the ionic nature of the TCNE−HMB complex over this pressure range.[60]

Large vibrational shifts are also calculated to occur for three out-of-plane HMB vibrations near 842, 856, and 1073 cm^{-1}. Confirmation of the shifts associated with these vibrations is not possible experimentally because of the low intensity. Several in-plane vibrations, which are calculated at 812, 878, 915, and 1050 cm^{-1} have an average vibrational shift of 20 cm^{-1}. Only the shift of the vibration at 1050 cm^{-1} can be confirmed experimentally.

Conclusions

Structural and molecular changes in the TCNE−HMB complex compressed to 0.417 GPa were investigated using neutron diffraction, inelastic neutron scattering, and quantum chemical calculations. Analysis of the neutron powder diffraction at 50 K indicated anisotropic compression of the *b* axis. The *b* axis lies perpendicular to the molecular stacks, which only interact by van der Waals forces, making it highly compressible. It is expected that the spacing between the molecular stacks will continue to decrease until dissociation begins at approximately 6 GPa.[44]

The very good frequency agreement between the observed and computed inelastic neutron scattering spectra implies that the computational methods used provide a reasonably accurate quantitative description of the TCNE−HMB complex as a function of pressure. Several vibrations with a large degree of methyl motion had calculated vibrational shifts of greater than 10 cm^{-1} over the pressure range studied. Unfortunately, in some cases, we were unable to experimentally confirm the vibrational shifts predicted by the calculations, due to poor resolution or low vibrational intensity. Infrared or Raman spectroscopy with less spectral congestion can perhaps be used to identify these shifts.

Although some vibrational peaks were not able to be experimentally resolved, there seems to be good reason to suggest that these computations are reliable. To improve the agreement between experiment and calculation, it will be necessary to perform more extensive solid-state calculations with the use of a supercell. However, from the degree of frequency agreement between the experimental and simulated INS spectra, we can imply that the molecular geometry must be qualitatively correct. We suggest that the large degree of errors observed in the lattice vectors have little effect on the overall molecular structure, but a definite conclusion as to this will require confirmation of the molecular positions, via single-crystal diffraction, as a function of pressure.

Acknowledgment. The NIST Center for Neutron Research is acknowledged for providing neutron beam access on the FANS and BT-1 instruments. The Army Research Laboratory Major Shared Resource Center is thanked for access and support of the VASP program. An NRC Fellowship with the Army Research Laboratory supported J.C. during the course of this research.

Supporting Information Available: Table S1 reports the estimated error in the lattice vectors and volume of the TCNE−HMB complex. This material is available free of charge via the Internet at http://pubs.acs.org.

References and Notes

(1) Miller, J. S.; Epstein, A. J. Molecule-based Magnets. In *Crystal Engineering: From Molecules and Crystals to Materials*; Braga, D., et al., Eds.; Kluwer: Dordrecht, The Netherlands, 1999; pp 43−53.

(2) Jerome, D.; Schultz, H. J. Organic conductors and superconductors. *Adv. Phys.* **2002**, *51*, 293.

(3) Singleton, J. *J. Solid State Chem.* **2002**, *168*, 689.

(4) Streetman, B.; Banarjee, S. *Solid State Electronic Devices*, 6th ed.; Prentice Hall: Englewood Cliffs, NJ, 2005.

(5) Freo, L. D.; Painelli, A.; Soos, Z. G. *Phys. Rev. Lett.* **2002**, *89*, 027402−1−4.

(6) Uno, B.; Okumura, N.; Seto, K. *J. Phys. Chem. A* **2000**, *104*, 3064.

(7) Tang, L.-T.; Wei, Y.; Wang, Y.; Hu, S.-W.; Liu, X.-Q.; Chu, T.-W.; Wang, X.-Y. *J. Mol. Struct. (THEOCHEM)* **2004**, *686*, 25.

(8) Oisen, V.; Rabiller, P.; Katan, C. *J. Phys. Chem. A* **2004**, *108*, 11049.

(9) Liao, M.-S.; Lu, Y.; Scheiner, S. *J. Comput. Chem.* **2002**, *24*, 624.

(10) Ciezak, J. A.; Hudson, B. S. *J. Mol. Struct. (THEOCHEM)* **2005**, *755*, 195.

(11) Sawka-Dobrowolska, W.; Bator, G.; Sobczyk, L.; Pawlukojc, A.; Ptasiewicz-Bak, H.; Rundlöf, H.; Krawczyk, J.; Nowina-Konopka, M.; Jagielski, P.; Janik, J. A.; Prager, M.; Steinsvoll, O.; Grech, E.; Nowicka-Scheibe, J. *J. Chem. Phys.* **2005**, *123*, 124305.

(12) Verdal, N.; Kozlowski, P. M.; Hudson, B. S. *J. Phys. Chem. A* **2005**, *109*, 5724.

(13) Hudson, B. S.; Allis, D. G.; Parker, S. F.; Ramirez-Cuesta, R. J.; Herman, H.; Prinzbach, H. *J. Phys. Chem. A* **2005**, *109*, 3418.

(14) Ciezak, J. A.; Trevino, S. F. *J. Mol. Struct. (THEOCHEM)* **2005**, *723*, 241.

(15) Plazanet, M.; Fontaine-Vive, F.; Gardner, K. H.; Forsyth, V. T.; Ivanov, A.; Ramirez-Cuesta, A. J.; Johnson, M. R. *J. Am. Chem. Soc.* **2005**, *127*, 6672.

(16) Eckert, J.; Sewell, T. D.; Kress, J. D.; Kober, E. M.; Wang, L. L.; Olah, G. *J. Phys. Chem. A* **2004**, *108*, 11369.

(17) Johnson, M. R.; Parlinski, K.; Natkaniec, I.; Hudson, B. S. *Chem. Phys.* **2003**, *291*, 53.

(18) Hermet, P.; Bantignies, J. L.; Rahmani, A.; Sauvajol, J. L.; Johnson, M. R. *J. Phys. Chem. A* **2005**, *109*, 4202.

(19) Hudson, B. S. *J. Phys. Chem. A* **2001**, *105*, 3949.

(20) Saheki, M.; Yamada, H.; Yoshioka, H.; Nakatsu, K. *Acta Crystallogr.* **1976**, *B32*, 662.

(21) Maverick, E.; Trueblood, K. N.; Bekoe, D. A. *Acta Crystallogr.* **1978**, *B34*, 2777.

(22) Forster, R.; Kulevsky, N. *J. Chem. Soc., Faraday Trans. 1* **1973**, *69*, 1927.

(23) Rossi, M.; Buser, U.; Haselbach, E. *Helv. Chim. Acta* **1976**, *59*, 1039.

(24) Liptay, W.; Rehm, T.; Wehnig, D.; Schanne, W.; Baumann, W.; Lang, W. *Z. Naturforsch. Teil A* **1982**, *37*, 1427.

(25) Stanley, J.; Smith, D.; Latimer, B.; Devlin, J. P. *J. Phys. Chem.* **1966**, *70*, 0, 2011.

(26) Hall, B.; Devlin, J. P. *J. Phys. Chem.* **1966**, *71*, 465.

(27) Sakehi, M.; Yamada, H. *Spectrochim. Acta* **1976**, *A32*, 1425.

(28) Rossi, M.; Haselbach, E. *Helv. Chim. Acta* **1979**, *62*, 140.

(29) Cesaro, S. N.; Martini, B.; Bencivenni, L.; Spoliti, M.; Maltese, M. *Spectrochim. Acta* **1980**, *A36*, 165.

(30) Yamamoto, K.; Kabit, Md. H.; Hayashi, M.; Tominaga, K. *Phys. Chem. Chem. Phys.* **2005**, *7*, 1945.

(31) Smith, M. L.; McHale, J. L. *J. Phys. Chem.* **1985**, *89*, 4002.

(32) McHale, J. L.; Merriam, M. J. *J. Phys. Chem.* **1989**, *93*, 526.

(33) Britt, B. M.; Lueck, H. B.; McHale, J. L. *Chem. Phys. Lett.* **1992**, *190*, 528.

(34) Britt, B. M.; McHale, J. L.; Friedrich, D. M. *J. Phys. Chem.* **1995**, *99*, 6347.

(35) Kulinowski, K.; Gould, I. R.; Meyers, A. B. *J. Phys. Chem.* **1995**, *99*, 9017.

(36) Britt, B. M.; McHale, J. L. *Chem. Phys. Lett.* **1997**, *270*, 551.

(37) Kulinowski, K.; Gould, I. R.; Ferris, N. S.; Meyers, A. B. *J. Phys. Chem.* **1995**, *99*, 17715.

(38) Hayashi, M.; Yang, T.-S.; Yu, J.; Mebel, A.; Lin, S. H. *J. Phys. Chem. A* **1997**, *101*, 4156.

(39) Gott, J. R.; Maisch, W. G. *J. Chem. Phys.* **1963**, *39*, 2229.

(40) Offen, H. W.; Kadhim, A. H. *J. Chem. Phys.* **1966**, *45*, 269.

(41) Nakayama, R.; Sasaki, M.; Osugi, A. *J. Rev. Phys. Chem. Jpn.* **1976**, *46*, 57.

(42) Ewald, A. H. *Trans. Faraday Soc.* **1968**, *64*, 733.

(43) Davis, K. M. C. In *Molecular Association*; Foster, R., Ed.; Academic: New York, 1975; Vol. 1, p 151.

(44) Jurgensen, C. W.; Peanasky, M. J.; Drickamer, H. G. *J. Chem. Phys.* **1985**, *83*, 6108.

(45) Yamada, H.; Saheki, M. *Spectrochim. Acta* **1980**, *37A*, 17.

(46) Byrd, E. F. C.; Scuseria, G. E.; Chabalowski, C. F. *J. Phys. Chem. B* **2004**, *108*, 13100.

(47) Details of the Harwood Engineering two-piston pressure intensifier system available for use at the NIST Center for Neutron Research can be found at http://users.rcn.com/harwood.ma.ultranet/prim200k.html.

(48) Specific instrumental details of the BT-1 powder diffractometer can be found at http://www.ncnr.nist.gov/instruments/bt1.

(49) Larson, A. C.; VonDreele, R. B. General Structure Analysis System (GSAS); Los Alamos National Laboratory Report LAUR 86-748; LANL: Los Alamos, NM, 2000.

(50) Toby, B. H. *J. Appl. Crystallogr.* **2001**, *34*, 210.

(51) (a) Udovic, T. J.; Neumann, D. A.; Leão, J.; Brown, C. M. *Nucl. Instrum. Methods Phys. Res.* **2004**, *A517*, 189. (b) www.ncnr.nist.gov/instruments/fans.

(52) http://www.ncnr.nist.gov/dave.

(53) Kresse, G.; Furthmuller, J. *Vienna Ab Initio Simulation Package (VASP): The Guide*; VASP Group, Institut fur Materialphysik, Universitat Wein, Sensengasse 8, A-1130 Wien, Vienna, Austria, 2003.

(54) Perdew, J. P.; Berke, K.; Ernzerhof, M. *Phys. Rev. Lett.* **1996**, *77*, 3865.

(55) Perdew, J. P. In *Electronic Structures of Solids '91*; Ziesche, P., Eschrig, H., Eds.; Akademie-Verlag: Berlin, 1991.

(56) Vanderbuilt, D. *Phys. Rev. B* **1990**, *41*, 7892.

(57) Ramirez-Cuesta, A. J. *Comput. Phys. Commun.* **2004**, *157*, 226.

(58) (a) Stride, J. A.; Adams, J. M.; Johnson, M. R. *Chem. Phys.* **2005**, *317*, 143. (b) Krawczyk, J.; Mayer, J.; Natkaniec, I.; Nowina Konopka, M.; Pawkukojc, A.; Steinsvoll, O.; Janik, J. A. *Physica B* **2005**, *362*, 271.

(59) (a) Torrance, J. B.; Girlando, A.; Mayerle, J. J.; Crowley, J. I.; Lee, V. Y.; Batail, P.; LaPlaca, S. J. *Phys. Rev. Lett.* **1981**, *47*, 1747. (b) Torrance, J. B.; Vazquez, J. E.; Mayerle, J. J.; Lee, V. Y. *Phys. Rev. Lett.* **1981**, *46*, 253.

(60) Moreac, A.; Girard, A.; Delugeard, Y.; Marqueton, Y. *J. Phys.: Condens. Matter* **1996**, *8*, 3553.